Nanochannel flow past permeable walls via molecular dynamics

Jian-Fei Xie and Bing-Yang Cao[a]
Key Laboratory for Thermal Science and Power Engineering of Ministry of Education and Department of Engineering Mechanics, Tsinghua University, Beijing 100084, China

(Received 20 April 2016; accepted 6 July 2016; published online 13 July 2016)

The nanochannel flow past permeable walls with nanopores is investigated by molecular dynamics (MD) simulations, including the density distribution, velocity field, molecular penetration mechanism and surface friction coefficient. A low density distribution has been found at the gas-wall interface demonstrating the low pressure region. In addition, there exists a jump of the gas density on the permeable surface, which indicates the discontinuity of the density distribution across the permeable surface. On the other hand, the nanoscale vortices are observed in nanopores of the permeable wall, and the reduced mass flux of the flow in nanopores results in a shifted hydrodynamic boundary above the permeable surface. Particularly the slip length of the gas flow on the permeable surface is pronounced a non-linear function of the molecular mean free path, which produces a large value of the tangential momentum accommodation coefficient (TMAC) and a big portion of the diffusive refection. Moreover, the gas-gas interaction and multi-collision among gas molecules may take place in nanopores, which contribute to large values of TMAC. Consequently the boundary friction coefficient on the permeable surface is increased because of the energy dissipation consumed by the nanoscale vortices in nanopores. The molecular boundary condition provides us with a new picture of the nanochannel flow past the permeable wall with nanopores. [http://dx.doi.org/10.1063/1.4959022]

I. INTRODUCTION

Micro/nano scale flow is of great significance in nanoscience and engineering such as in micro/nano-electromechanical systems (MEMS/NEMS),[1–5] Lab-on-a-Chip[6–8] and micro-total-analysis systems (μTAS).[9–11] One of the most important assumptions for flow past solid walls is the no-slip boundary condition (NSBC), which indicates that the fluid elements attached to the solids assume the velocity of the surface.[12] Although traditionally macroscopic studies have a good agreement with this NSBC, recent work has investigated the micro/nano flow from the molecular point of view showing that the NSBC may be different.[13] Therefore, a deep understanding of the micro/nano flows seems essential to both theoretical study and engineering applications. One of the most important issues in flow development at the micro/nano scale is the velocity slip on the boundary,[12–17] and the Navier slip boundary condition (SBC) illustrates that the slip length L_s can be expressed by the slip velocity u_s and the local shear rate $\partial u/\partial z$ as follows

$$L_s = \frac{u_s}{\partial u/\partial z|_{z=0}}. \tag{1}$$

Note that the wall is located at $z = 0$. Additionally, the dimensionless slip length ($l_s = L_s/H$ where H is the characteristic length of the flow geometry) that is relevant to the Knudsen number

[a]caoby@tsinghua.edu.cn

($Kn = \lambda/H$ where λ is the molecular mean free path) can be predicted by Maxwell theory

$$l_s = \frac{2-\varsigma}{\varsigma} Kn, \tag{2}$$

in which ς is the tangential momentum accommodation coefficient (TMAC) indicating the percentage of gas molecules that have been bounced back diffusively from the solid wall. It is obvious that Maxwell theory always indicates a positive slip length for the rarefied gas flow.[18]

Apart from the flow past the smooth solid wall, flows in complex geometries with porous walls are also of great importance to engineering and science. For example, channel flows past porous walls, which are called Berman flows,[19,20] have been applied to modelling the membrane separation processes,[21] particle filtration[22] and biomedical transport phenomena. When the viscous Newtonian fluid flows past a porous wall, the NSBC is usually applied to explain the momentum exchanges within the porous walls and the flow velocity has always been assumed to be that of the solid surface. However, there is no guarantee that the NSBC is still suitable for the flow past a permeable surface. Beavers and Joseph had pointed out that the NSBC cannot be used on the permeable boundary since there existed a momentum transfer inducing the slip velocity on the porous wall having large open pores.[23,24] On the other hand, the velocity slip also occurs in porous media such as the brine water and supercritical CO_2 flow in nanopores of sandstone rocks, and it is necessary to consider the SBC for the fluid flow in microporous media.[25–31] In addition, we compare the fluid flow past the porous wall with the one past a rough wall. Much work has been done to study the influence of wall roughness on the channel flows, including the rectangular, sinusoidal, triangular[32–34] and topological surfaces.[35] The fluid occupied the space of wall roughness without moving and its influence on the bulk flow can be ignored.[33] The permeable surface, however, displays absolutely different pictures that the fluid can penetrate the permeable surface and flow into the micro/nanopores. In this case, the assumption that the fluid molecules will be bounced back on the solid wall when they impinge on the wall breaks down and Maxwell theory is not suitable for the predict of TMAC on the permeable surface. Therefore, much attention needs to be paid to identify the tangential component of the flow velocity on the porous wall, and a preferable molecular boundary condition is desirable.

For fluid flow bounded by porous walls, the SBC has been employed on the surface of the porous medium. For example, Sparrow and Beavers had obtained the velocity distributions for rectangular ducts bounded by one porous wall and estimated the friction coefficients on the porous wall.[36] However, the fluid properties such as the density distribution and the velocity at the fluid-wall interface have not been investigated, and the fluid dynamics past the permeable walls have not been well understood either. There are two typical particle-based approaches to modelling micro/nanoscale fluid flows, i.e. direction simulation Monte Carlo (DSMC)[37,38] and molecular dynamics (MD) simulations.[39] DSMC has been always preferred due to its high efficiency and low computational cost. However, the modelled boundary condition and simplified fluid-wall interaction make DSMC not to precisely describe the flow around the complex geometries and flow fields with vortices.[40,41] MD simulations can provide the accurate description of boundary condition at the molecular level and determination of gas-wall interactions. The purpose of this paper is to investigate the effect of the porous wall having nanopores on the nanochannel flow via MD simulations, and the next section is followed by the nanochannel flow details and MD techniques. Sec. III shows MD simulation results, including the density distribution, velocity field, the molecular behaviours in nanopores of the permeable walls and the boundary friction coefficient. Conclusions are drawn in Sec. IV.

II. MOLECULAR DYNAMICS SIMULATIONS

A three-dimensional gas Couette flow was performed: the gas molecules were confined between two solid planes parallel to each other, as shown in Fig. 1(a). The upper wall was moved by a constant velocity of u_0 along the x direction and a stationary wall was placed on the bottom. In addition, periodic boundary condition was applied to the x and y directions for the gas flow. Wall atoms were set to the face-centred-cubic (f.c.c) lattice sites, and based on the Einstein theory

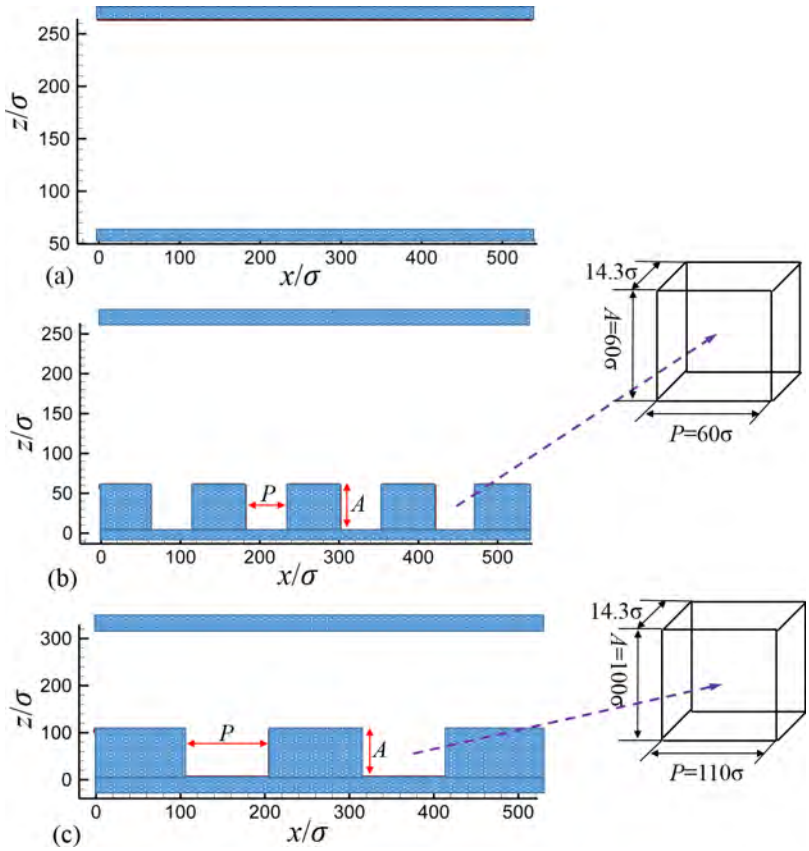

FIG. 1. Nanochannel geometry: (a) two smooth walls with height $H = 205\sigma$; (b) a permeable bottom wall with height $H = 205\sigma$, nanopores $A = 60\sigma$ and $P = 60\sigma$; and (c) a permeable bottom wall with height $H = 205\sigma$, nanopores $A = 100\sigma$ and $P = 110\sigma$. The y direction points into the $x - z$ plane and the length of cell in the y direction is $L_y = 14.3\sigma$ for all three nanochannels.

each wall atom vibrated around the f.c.c lattice site with the Einstein frequency by a harmonic spring with stiffness $k = 16\pi^4 k_B^2 m\theta^2/\hbar^2$, where k_B and $\hbar$ are the Boltzmann and Plank constants, m is the mass of a wall atom, and θ =180 K is the Einstein temperature.[18] Note that there is an errata Einstein frequency in Eq. (1) of Ref. 18 and the temperature should be squared instead of the mass of wall atom. The gas in the nanochannel was driven to be a laminar flow. The simulated characteristic length from the surface of bottom wall to the upper wall, i.e., the effective height of the nanochannel, reaches $H = 205\sigma$ which is in the range of the characteristic length of NEMS devices. The sizes of the simulation cell in the x and y directions are about $L_x = 520 \sim 540\sigma$ and $L_y = 14.3\sigma$, respectively. Besides the smooth wall, the permeable walls were also considered in our MD simulations, which are shown in Figs. 1(b) and 1(c). The permeable walls can be expressed as porosity having nanopores, which are parameterized using an amplitude A and a space P. Two types of permeable walls were considered, i.e., one has the nanopores of $A = 60\sigma$ and $P = 60\sigma$, and the other of $A = 100\sigma$ and $P = 110\sigma$. It should be pointed out that the size of nanopores is much larger than the amplitude of the roughness ($\sim 10\sigma$) and is the same order as the molecular mean free path or larger. Both magnitudes of nanopores can guarantee that the gas flow in nanochannels with the permeable wall is completely different from the one past the rough surface.

Intermolecular interactions between gas molecules are calculated using the Lennard-Jones (L-J) 12-6 potential

$$\phi(r) = 4\varepsilon[(\frac{\sigma}{r})^{12} - (\frac{\sigma}{r})^{6}], \tag{3}$$

where r is the distance between two gas molecules, ε and σ are the strength of interaction and length scale, respectively. As the argon molecules are used, $\sigma_A = 3.405 \times 10^{-10}$ m is chosen as a length scale and $\varepsilon_A = 1.67 \times 10^{-21}$ J is used as an energy magnitude. Moreover, $\sigma_{AP} = 3.085 \times 10^{10}$ m and $\varepsilon_{AP} = 0.894 \times 10^{-21}$ J are taken for the argon-platinum (gas-wall) interactions that are represented as follows

$$\phi(r)_{AP} = 4\varepsilon_{AP}[(\frac{\sigma_{AP}}{r})^{12} - (\frac{\sigma_{AP}}{r})^{6}]. \tag{4}$$

The molecular mass is $m_A = 40$ a.u for argon and $m_P = 195$ a.u. for platinum, and the running time scale in MD simulations is specified as $\tau = \sigma_A\sqrt{m_A/\varepsilon_A} = 2.15 \times 10^{-12}$ s. The upper wall was moved by a velocity of $u_0 = 1.0\sigma_A/\tau$.

The equation of motion of gas molecules was solved numerically in terms of the leapfrog Verlet algorithm with a time step of $\Delta t = 0.02\tau$. Besides, to reduce the computational cost by computing the intermolecular interactions, two main techniques were taken: a typical potential cutoff of $r_{cut} = 2.5\sigma$ that is close to the one applied to the dilute gas and the cell-linked list method.[39] A larger cut-off distance may be needed, but it will not affect the density calculations for L-J fluids. It must be noted that long-range attractive interactions between molecules may be applied to accurately calculate the dense gas and liquid pressure.[42] The gas and wall temperatures were both set as $T = 119.8$ K. Based on the phase diagram,[14] the number density of gas molecules is in the range of $0.007 \sim 0.044$ with the temperature to ensure the gaseous state of argon in our investigations. On the basis of the kinetic theory, the mean free path of gas molecules can be estimated varying from 7.3σ to 26.2σ via a hard-sphere gas model.[15] The motion equation of the ith gas molecule is given by

$$m\frac{dz_i^2}{dt^2} = \sum_{j\neq i}\frac{\partial\phi_{LJ}}{\partial z_i} - m\Gamma\dot{z}_i + \eta_i, \tag{5}$$

in which Γ is a friction factor that is used to specify the heat transfer rate between gas and the heat bath, and η_i is a random force that is applied to reduce the statistical fluctuation and has the Gaussian distribution.[43] In order to remove the viscous heat produced by the gas flow, a Langevin thermostat technique[44] was adopted along the nanochannel height to keep the gas temperature constant and ensure an isothermal process. The wall temperature was maintained unchanged by applying the velocity rescaling approach to wall atoms. Typically one million time steps were required to approach a steady gas flow, and additional 1,500,000 time steps were needed to obtain the macroscopic characteristics.

III. RESULTS AND DISCUSSION

A. Gas density profiles

The three-dimensional steady gas flows in the three nanochannels are shown in Fig. 2. It displays that the gas flows in the whole nanochannels under the shearing of the top wall and the gas molecules drop into the nanopores by penetrating the permeable surface when the flow systems reach the equilibrium state. Density contour of the gas flow in the three nanochannels is shown in Fig. 3. The following discussions of our MD simulations are based on the same gas rarefication, i.e. the Knudsen number is fixed. Because of the extra room added by nanopores in nanochannels with the permeable surface, the number of gas molecules is increased slightly in amount. The density distribution is more uniform in the nanochannel with the smooth surface as shown in Fig. 3(a), but the density distribution in the nanopores is the lower than that in the bulk region of the nanochannels with permeable surfaces as shown in Figs. 3(b) and 3(c). Further, a low density distribution is found near the solid wall in the nanochannels whatever the wall is smooth or permeable. For example, we zoom into the gas-wall interface in the nanopores of the permeable walls as shown in Figs. 3(b) and 3(c) and find that the density at the gas-wall interface is lower than that in the bulk region of the nanochannel. The low gas density near the wall surface is caused by the weak gas-wall interaction indicating the hydrophobic characteristics. Based on the equation of state, we can conclude that a

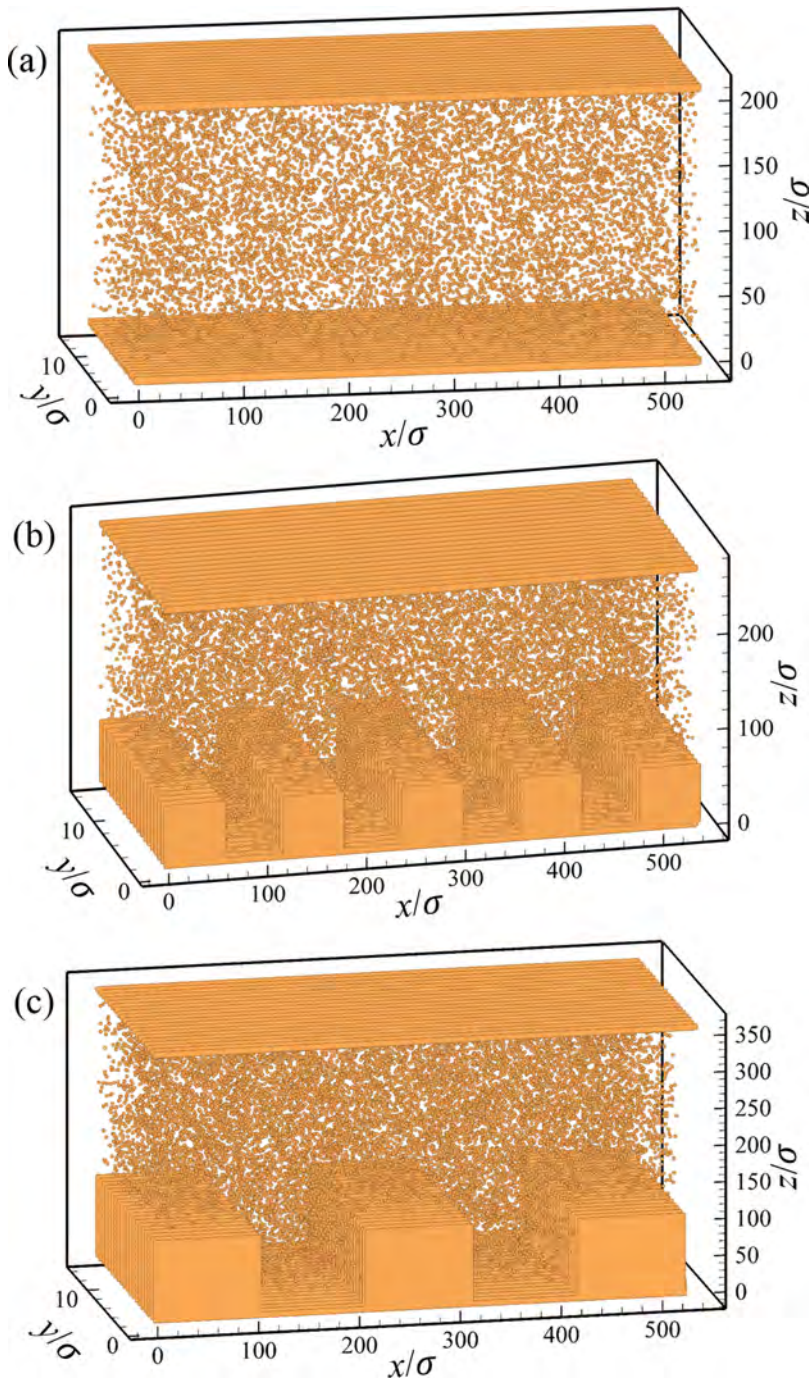

FIG. 2. Snapshots of gas nanohannel flow past: (a) a smooth wall; (b) a permeable bottom wall with nanopores $A = 60\sigma$ and $P = 60\sigma$; and (c) a permeable bottom wall with nanopores $A = 100\sigma$ and $P = 110\sigma$. The moving velocity of the upper wall is fixed as u_0 and the directions are the same as Fig. 1.

low gas density distribution near the solid wall will result in a low gas pressure contribution at the gas-wall interface. Due to the non-thermodynamic state of gas near the solid wall, however, the law breaks down and the gas pressure should be computed using the Irving-Kirkwood method.[45] In addition, the inclusion of gas-wall virial indicates that the gas pressure cannot be calculated exactly near the solid wall, because the three mutually orthogonal components of the stress tensor are anisotropic.[42] To ensure the isothermal process during the MD runs, gas and wall temperatures

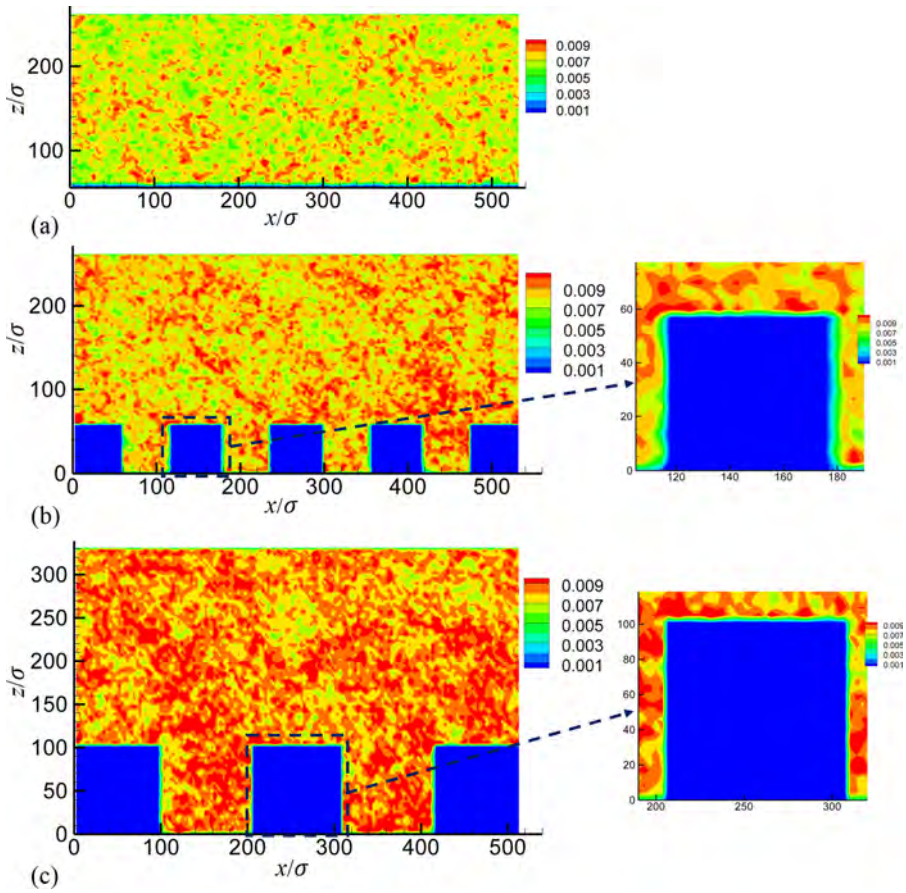

FIG. 3. Density contour of the gas flow past: (a) a smooth wall; (b) a permeable bottom wall with nanopores $A = 60\sigma$ and $P = 60\sigma$; and (c) a permeable bottom wall with nanopores $A = 100\sigma$ and $P = 110\sigma$. The blue squares are the solid parts of the nanochannels.

are monitored. It can be seen in Fig. 4 that both temperatures almost keep the same level showing no big deviation from the initial setup.

We look at the density profiles of the gas flow across the nanochannels, i.e., along the height of the nanochannels, as shown in Fig. 5. For the nanochannel with the smooth surface (indicated by the

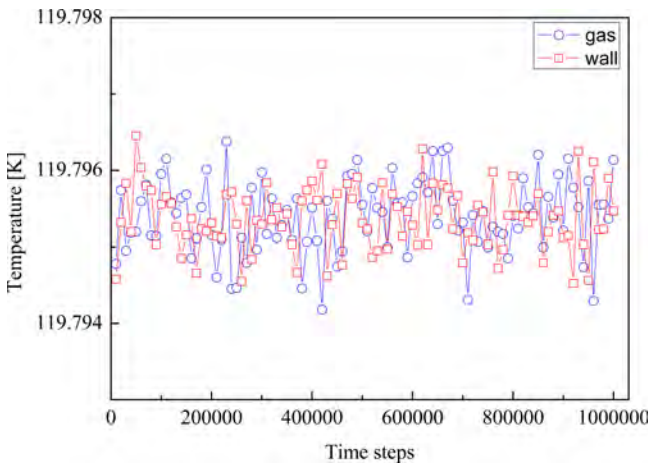

FIG. 4. Historical diagram of gas and wall temperatures in MD simulations.

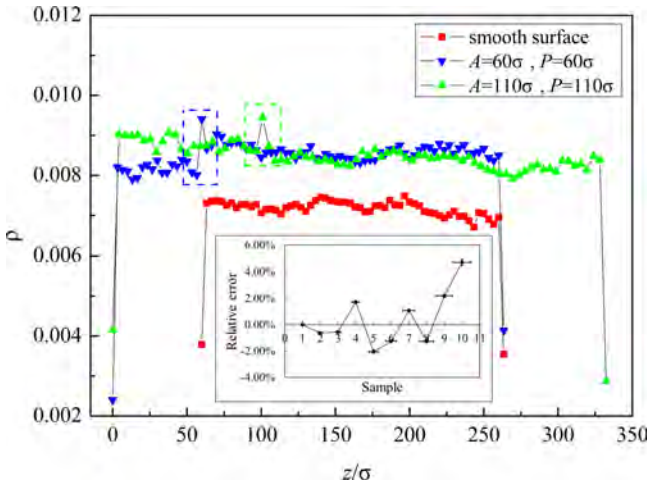

FIG. 5. Density profiles of the gas flow past: a smooth wall (red squares); a permeable bottom wall with nanopores $A = 60\sigma$ and $P = 60\sigma$ (blue inverted triangles); and a permeable bottom wall with nanopores $A = 100\sigma$ and $P = 110\sigma$ (green triangles).

red squares), the density of gas molecules keeps about 0.07 in the bulk region of the nanochannel. However, the gas density is sharply decreased at the gas-wall interface and drops to 0.004. For the nanochannel with the permeable surface having small nanopores (indicated by the blue inverted triangles), the density of gas molecules in the nanopores is obviously lower than that in the bulk region, and the gas density at the gas-wall interface also drops down, which is much lower than both in the nanopores and bulk region. Particularly there is a jump of the gas density for the permeable surface at $z = 60\sigma$ (indicated by a blue dotted square), which is slightly larger than the bulk density. For the nanochannel with the permeable surface having large nanopores (indicated by the green triangles), the density of gas molecules in the nanopores keeps the same level as that in the bulk region. This can be explained that the gas molecules can enter the large nanopores more easily compared to the small ones. It means that large nanopores can capture more gas molecules and the statistical property of the gas density in nanopores is closer to the macroscopic level. There is also a jump of the gas density for the permeable surface at $z = 100\sigma$ (indicated by a green dotted square) where the gas density is a bit larger than that in the bulk region. The jump of the gas density on the permeable surface can be seen a "switch" when the gas molecules penetrate the permeable surface. The blocking of the gas molecules by the "switch" results in a jump of the gas density on the permeable surface. The trapping of gas molecules in nanopores functioning as a switch on the permeable surface increases the probability of collisions between gas molecules and resists the dropping of other gas molecules from the bulk region. As a result, the gas density is plumped up on the permeable surface resulting in a jump. The gas density drop at the gas-wall interface is consistent with the lower density near the solid wall observed in Fig. 3. In order to ensure that the density jump is physical and is not caused by the statistical scatter in MD simulations, the relative error between the averaged samples has been also shown in Fig. 5. It can be seen that the relative error is less than 5.0% indicating the physical jump of gas density on the permeable surface.

B. Velocity profiles and slip length

The permeable surface will influence the gas flow past it and the velocity fields of the gas flow past different wall surfaces are shown in Fig. 6. As shown in Fig. 6(a), the streamline of the gas flow in the bulk region of the nanochannel with the smooth surface is uniform under the shearing of the top wall but the flow is disturbed up to about 20σ away from the solid bottom wall. When the gas flows past the permeable surface having small nanopores, as shown in Fig. 6(b), the gas flows into the nanopores and produces several nanoscale vortices in each nanopore. Compared to the smooth surface, the gas flow is disturbed up to about 40σ away from the permeable surface. When the

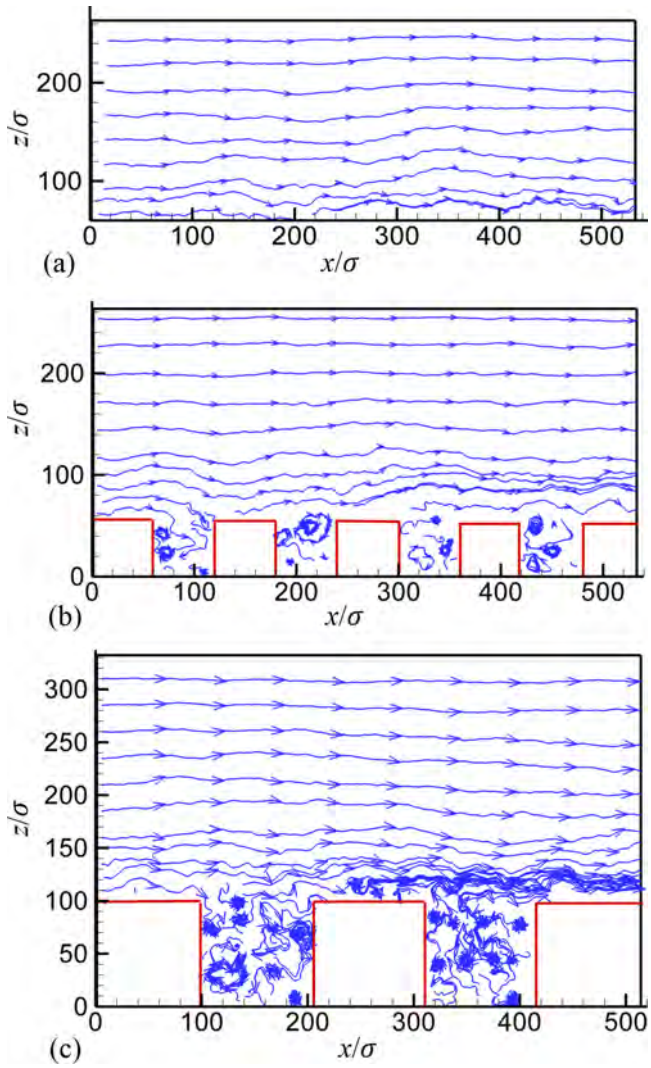

FIG. 6. Velocity field of the gas flow past: (a) a smooth wall; (b) a permeable bottom wall with nanopores $A = 60\sigma$ and $P = 60\sigma$; and (c) a permeable bottom wall with nanopores $A = 100\sigma$ and $P = 110\sigma$. The red solid lines are the boundaries of the permeable surface.

gas flows past the permeable surface having large nanopores, as shown in Fig. 6(c), there are more nanoscale vortices produced in each large nanopore in comparison with the small nanopores shown in Fig. 6(b) and the gas flow is disturbed up to about 50σ away from the permeable surface. For gas flow in microchannels, it was observed that the streamlines near the rough surface are obviously distorted and are expanded between rough elements.[33] For nanochannels with the large roughness surface, Sun *et al*. had observed the closed streamline circles in the centre of concave,[46] which indicates that the free molecular motion can form a steady vortex. For the electroosmotic flows, the vortex was also reported in a channel with rectangle-waved surface roughness,[47] and the energy loss of the fluid flow in the rough-wall nanochannel had been found dependent on the channel geometrical characteristics.[48] As mentioned earlier, the size of nanopores in the nanochannel is larger than the mean free path of gas molecules, which allows sufficient intermolecular collisions, and one believes that nanoscale vortices are realistically produced. Therefore, we can conclude that the gas flow in the bulk region of the nanochannel is disturbed more easily by the permeable surface compared to the smooth surface and the permeable surface having large nanopores influences the gas flow more significantly. In addition, we focus on the gas flow in the nanopores finding that the gas flow gets disorder due to the nanoscale vortices produced in nanopores and it becomes more

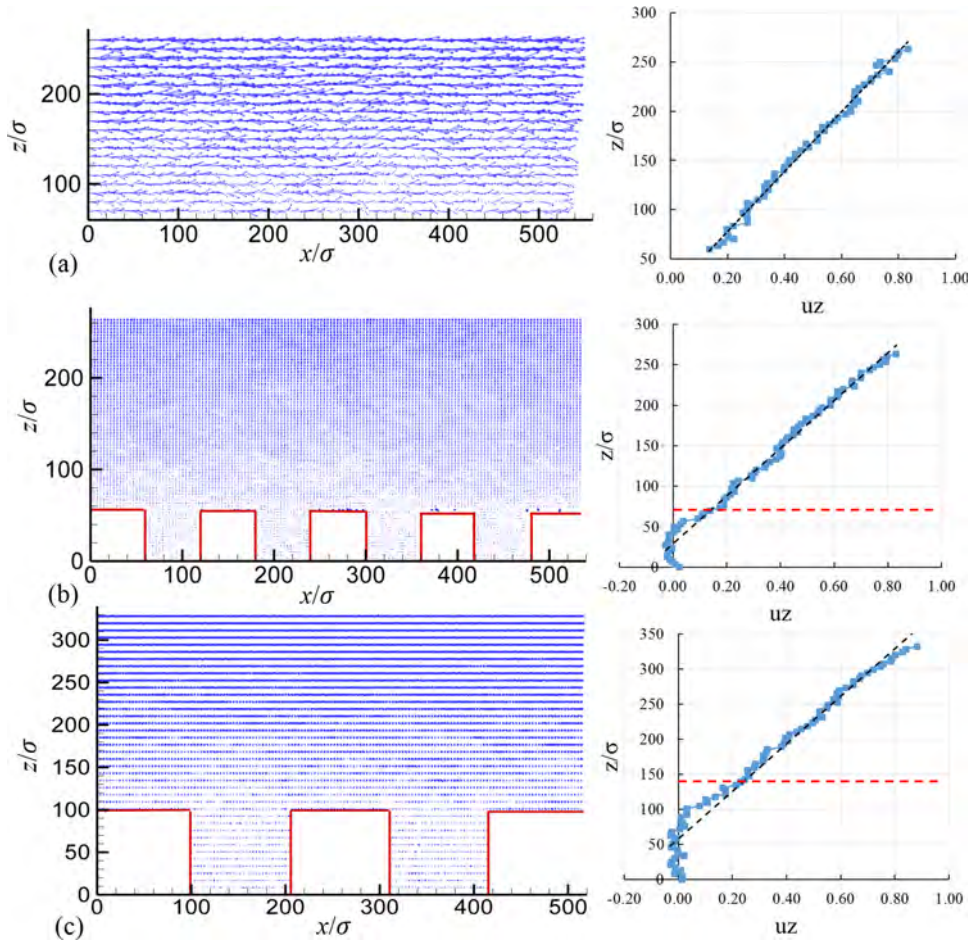

FIG. 7. Left panel: mass flux ($\rho\mathbf{u}$) of the gas flow past: (a) a smooth wall; (b) a permeable bottom wall with nanopores $A = 60\sigma$ and $P = 60\sigma$; and (c) a permeable bottom wall with nanopores $A = 100\sigma$ and $P = 110\sigma$. The red solid lines are the boundaries of the permeable surface. Right panel: velocity profiles related to the mass flux. The red dotted line indicates the shifted hydrodynamic boundary, and the black dotted line is the fit of the velocity profile.

disorder in large nanopores. Particularly the nanoscale vortices in the pores will result in the energy dissipation of the gas flow past the permeable surfaces.

The dynamics of gas molecules in the nanopores is different from that in the bulk region of nanochannels, and the mass flux ($\rho\mathbf{u}$) of gas flow across the nanochannels is shown in Fig. 7. As shown in Fig. 7(a), the mass flux of gas flow is uniform across the nanochannel with the smooth surface and the velocity profile is linear across the nanochannel. However, as shown in Fig. 7(b), the mass flux of gas flow in small nanopores is decreased for the permeable surface, and the velocity profile deviates from the linear portion at $z = 70\sigma$ (indicated by the red dotted line) which is higher than the height of small nanopores ($z = 60\sigma$). As shown in Fig. 7(c), the mass flux of gas flow in the large nanopores is also decreased for the permeable surface, and the velocity profile deviates from the linear portion further at $z = 140\sigma$ (indicated by the red dotted line) which is much higher than the height of large nanopores ($z = 100\sigma$). Both positions of the deviation from the height of nanopores occurred at the permeable surfaces are higher than the height of nanopores, i.e., $A = 60\sigma$ and $A = 100\sigma$, and the deviation happens furthest away from the permeable surface having large nanopores compared to the permeable surface having small ones. Tretyakov and Müller had also observed the reduction of the mass flux of a polymer liquid flow past patterned surfaces, and pointed out that the deviation of the velocity profile from the macroscopic fit began at the vicinity of the hydrodynamic boundary position.[49] In addition, we focus on the velocity profile of the gas flow in nanopores and find that the flow velocity fluctuates, which illustrates that the gas flows randomly in

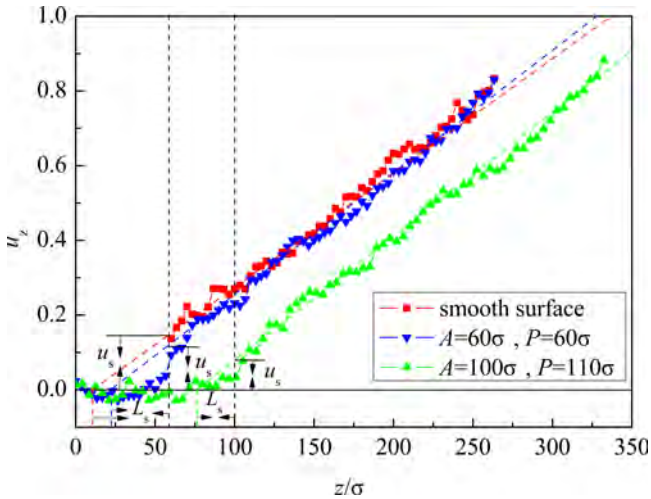

FIG. 8. Velocity profiles of the gas flow past: a smooth wall (red squares); a permeable bottom wall with nanopores $A = 60\sigma$ and $P = 60\sigma$ (blue inverted triangles); and a permeable bottom wall with nanopores $A = 100\sigma$ and $P = 110\sigma$ (green triangles). The two vertical dotted lines indicate the heights of small (left) and large (right) nanopores of nanochannels, respectively. The three diagonal dotted lines are the fitting of the velocity profiles across the nanochannels with the smooth surface (red), the permeable surface with small nanopores (blue) and the permeable surface with large nanopores (green) separately.

nanopores and is consistent with the appearance of nanoscale vortices observed in Fig. 6. The above observations indicate that the hydrodynamic position for the gas flow has been shifted above the permeable surface, which may influence the local shear rate and the effective boundary properties.

We now focus on the velocity profiles across the nanochannels, which are shown in Fig. 8. For the smooth surface (indicated by the red squares), the velocity profile is linear across the nanochannel and the velocity slip occurs on the smooth solid wall. For the permeable surface with small nanopores (indicated by the blue inverted triangles), the velocity profile in the bulk region of the nanochannel is close to that of the smooth surface and the velocity slip also occurs. However, the velocity profile drops down significantly in nanopores, and the whole velocity profile across the nanochannel shows a "spoon" configuration. For the permeable surface with large nanopores (indicated by the green triangles), the velocity profile of the gas flow deviates from both of the smooth surface and the permeable surface with small nanopores, and it also shows the "spoon" configuration. Apart from the velocity slip on the permeable surface, the gas flow fluctuates more significantly in large nanopores compared to the small ones. As seen in Fig. 6(c), more nanoscale vortices are produced in large nanopores, which results in the significant fluctuation of the gas flow in large nanopores. The two vertical dotted lines are used to indicate the height of nanopores on the permeable surfaces, which refers to the small nanopore $A = 60\sigma$ (left dotted line) and the large nanopore $A = 100\sigma$ (right dotted line), respectively. The slip velocity u_s on the smooth wall is larger than those on the porous walls. In addition, the slip length L_s on the permeable surface is smaller than that on the smooth surface, and it is decreased further on the permeable surface with $A = 100\sigma$. It had been also reported that the slip length on a rough surface decreased as the roughness increasing in the rough-wall nanochannel flow,[16,33] and Yang further pointed out that the presence of surface roughness always suppresses the slip length of fluid past the wall of nanochannels whatever the surface is hydrophilic or hydrophobic.[32] Moreover, Sokhan and Quirke found the slip length dependent sufficiently on the pore size and keeping a constant for pore size larger than 20σ,[50] which differs from the linear prediction by Maxwell slip theory. According to the mass flux shown in Fig. 7, we know that the hydrodynamic boundary has been shifted above the permeable surface and it is higher than the height of nanopores. Therefore, it can be concluded that the permeable gas-wall condition plays an important role in permeable-wall nanochannel flows.

The three diagonal dotted lines shown in Fig. 8 are the fits of the velocity profiles across the nanochannels with smooth and permeable surfaces, and the blue and green dotted lines illustrate

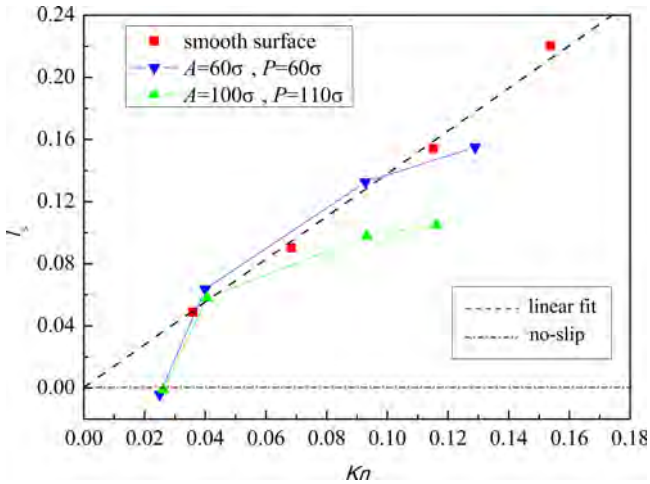

FIG. 9. Slip length L_s varied as a function of Kn when the gas flowed past: a smooth wall (red squares); a permeable bottom wall with nanopores $A = 60\sigma$ and $P = 60\sigma$ (blue inverted triangles); and a permeable bottom wall with nanopores $A = 100\sigma$ and $P = 110\sigma$ (green triangles).

that the slip velocity and slip length are influenced significantly by the permeable surfaces. On the basis of Navier SBC, the slip length L_s can be computed using Eq. (1) and the dimensionless slip length l_s is plotted as a function of Kn in Fig. 9. Kn varies as the gas density at the fixed nanochannel height. Note that MD simulations must be carried out in a domain that is greater than the mean free path of gas molecules to allow molecular collisions. The lateral dimension, however, i.e. $L_y = 14.3\sigma$, is smaller than the mean free path at large Kn. In this case, the simulations can be seen as quasi-three dimensional ones. The dimensionless l_s, as shown in Fig. 9, is an increasing function of Kn. As the slip length varies as the molecular mean free path, and we can rewrite Eq. (2) as follows

$$l_s = \alpha Kn, \tag{6}$$

in which α is the slip coefficient and we have $\alpha = (2 - \varsigma)/\varsigma$. Based on Maxwell theory, i.e., Eq. (6), one knows that the dimensionless slip length l_s is proportional linearly to Kn and the slip coefficient α is independent of Kn. On the other hand, the TMAC (ς) varies as solid surface conditions and ranges from zero to unity.[33] Thus, for a given gas-solid condition the slip coefficient is larger than unity numerically. The dimensionless slip length l_s on the smooth surface, as shown in Fig. 9, varies as a linear function of Kn, which reaches an agreement with the prediction of Maxwell theory, and we obtain $\varsigma = 0.82$ and $\alpha = 1.1$, respectively. However, as indicated by the inverted blue triangles and green triangles in Fig. 9, the dimensionless slip length l_s on the permeable surface is not a linear function of Kn, and the non-Maxwell slippage occurs. As a result, the TMAC (ς) on the permeable surface may be greater than unity for large Kn, which indicates that Maxwell theory fails to predict the slip length of the gas flow past a permeable surface and the TMAC (ς) is not limited to the range of $0 \sim 1.0$ for the permeable gas-solid condition. For example, comparing with the experimental results, Finger *et al.* found that the TMAC (ς) can be greater than unity because of the backscattering of reflected gas molecules on the solid surface.[51] It can be also seen in Fig. 9 that the slip length on the permeable surface is smaller than that on the smooth surface, and even the negative slip appears on the permeable surface for small Kn. Sun *et al.* also reported that the fluid molecules that can be firmly trapped in the concaves due to the rough surface and strong fluid-wall interaction may cause locking boundary in the velocity profile.[46]

C. Molecular behaviour inside porous walls

The gas molecules are bounced back diffusively when they impinge on a smooth solid wall. However, the gas molecules may cross the permeable surface and stay inside the nanopores if the

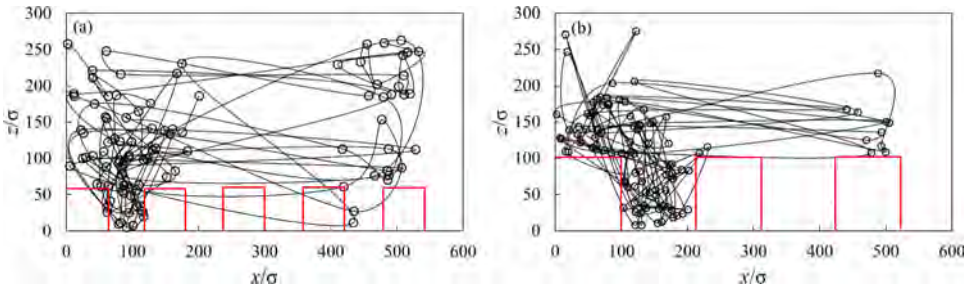

FIG. 10. Molecular trajectory indicated by the open circles when a gas molecule travelled in the nanochannel with nanopores: (a) $A = 60\sigma$ and $P = 60\sigma$ and (b) $A = 100\sigma$ and $P = 110\sigma$. The red solid lines are the boundaries of the permeable surface.

wall surface is permeable. For example, the gas flows in the nanochannels with the permeable surfaces having nanopores: (i) $A = 60\sigma$ and $P = 60\sigma$; (ii) $A = 100\sigma$ and $P = 110\sigma$, and we are concerned about the molecular behaviour inside the permeable walls. The molecular trajectory can draw a historical picture of the molecular movement of gas molecules confined between the plates and we thus track the trajectories of gas molecules while carrying out the MD simulations. As shown in Figs. 10(a) and 10(b), the gas molecule dropped into the nanopore and stayed for a period of time. Afterwards it escaped from that nanopore and travelled in the bulk region of the nanochannel for another period of time. Interestingly the molecule entered another nanopore later. For gas flow in microchannels with rectangular roughness, it was reported that the gas has no macroscopic velocity along the flow direction in the space between roughness units and the space is dead zones.[33] In addition, for stronger fluid-wall interactions in nanochannels Sofos *et al*. pointed out that liquid argon molecules can be trapped and stay for a longer time inside the cavity of a rough wall as the length of the protrusions decreases.[16] However, we find that there is no one gas molecule that can be trapped and reside in the nanopore all the time whatever the nanopore is small or large. This observation illustrates that the gas molecules travel all the time in the nanochannel even they enter the nanopores more than one time when the gas flows past the permeable surface. It also provides us with a picture that the gas flow in nanopores is not rest and influences the macroscopic flow, which is completely different from the fluid flow past a rough wall where the molecules are trapped in the rough space and there is no contribution to the macroscopic flow.[16,33] The molecule-trapped behaviour also occurred at the vapour-liquid interface of chain-like hydrogen molecules during the evaporation and condensation processes.[52] Li *et al*. had also investigated the flow penetration on the rough surface using a microporous model and found that the penetration depends on the porosity of the microporous media and plays an important role on the flow past a rough wall.[53]

Moreover, we record the frequency of gas molecules entering the small and large nanopores, respectively. Note that we colour the gas molecules that drop into nanopores at the very beginning of our MD simulations and record their trajectories till the end of simulations. Then the average time of the gas molecules that entered nanopores once is extracted, and each gas molecule has been tracked for 2,500,000 time steps totally. As shown in Fig. 11, the distribution of gas molecules dropped into nanopores of the nanochannels indicates that a large number of gas molecules enter the small nanopore less than 10 times. However, the number of gas molecules entering the small nanopore more than 15 times is sharply decreased. On the other hand, the number of gas molecules entering the large nanopore less than 10 times is decreased compared to the small nanopore. But the number of gas molecules entering the large nanopore more than 15 times is increased. In addition, very few gas molecules can enter nanopores up to 25 times whatever the nanopore is small or large. The gas molecules that dropped into nanopores by penetrating the permeable surface contribute to the large value of the TMAC (ς) that is greater than unity, which indicates that the diffusive reflection has been enhanced significantly on the permeable surface. In addition, it illustrates that the multi-collisions may take place among the gas molecules in nanopores when they penetrate the permeable surface and the momentum exchange happens not only between the gas molecules and wall atoms but also between gas molecules themselves in nanopores. Sun *et al*. also concluded that the liquid molecules had been trapped within the concave not only by the geometric conditions of

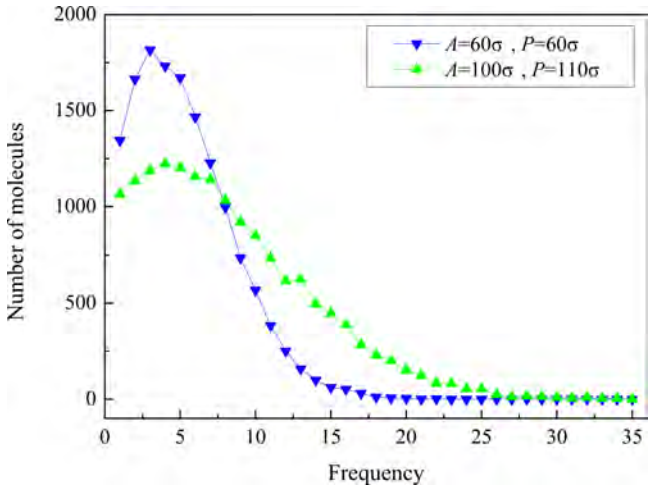

FIG. 11. Distribution of gas molecules dropped into nanopores of the nanochannel with nanopores: $A = 60\sigma$ and $P = 60\sigma$ (blue inverted triangles) and $A = 100\sigma$ and $P = 110\sigma$ (green triangles).

the roughness but also by the molecular interaction.[46] This molecular mechanism of momentum exchange in nanopores while the gas flow past a permeable surface will play an important role in the fluid-solid interfacial phenomena and affect the tangential momentum accommodation of gas flow in nanochannels having nanopores. We can conclude that the molecular behaviours combining multi-collisions and surface permeability are responsible to the induced non-Maxwell slippage on the permeable surface observed in Fig. 9. Therefore, the boundary condition on the smooth surface predicted by Maxwell theory is no longer valid to specify the tangential component of the fluid velocity on a permeable surface. Eventually a novel molecular boundary condition is desirable for the fluid flow past the permeable wall.

D. Boundary friction coefficient

The slip boundary condition has been affected by the permeable surface significantly when the gas flows past the porous wall, and we consider another boundary condition on the permeable surface. Generally the skin friction of a solid wall will be decreased if the slip velocity occurs on the surface. However, the fundamental of the friction is a lack of understanding when the fluid flows past the permeable surface. Thus we are to determine the surface friction of the gas flow on the permeable surface. For the laminar gas flow in nanochannels, the friction coefficient f is defined as

$$f = \frac{\tau_w}{\frac{1}{2}\rho u_0^2}, \tag{7}$$

where τ_w is the wall shear stress that is calculated by the net change of momentum of gas molecules on the wall per unit area and time using the Irving-Kirkwood express.[45] Usually a normalized friction constant C^* is used and given by

$$C^* = \frac{1}{1 + 6\frac{2-\varsigma}{\varsigma}Kn} = \frac{1}{1 + 6l_s}. \tag{8}$$

The friction coefficient C^* on the smooth and permeable surfaces as a function of Kn is plotted in Fig. 12. As shown in Fig. 12, the friction coefficient C^* is a decreasing function of Kn, and C^* on the permeable surface is larger than that on the smooth surface. The slip length on the permeable surface is smaller than that on the smooth surface in the slip region, which was illustrated in Fig. 9, and in turn, the smaller slip length on the permeable surface produces a larger friction coefficient in this region. It indicates that the larger friction coefficient on the permeable surface predicted in Fig. 12 is consistent with the smaller slip length on the permeable surface observed in Fig. 9. In

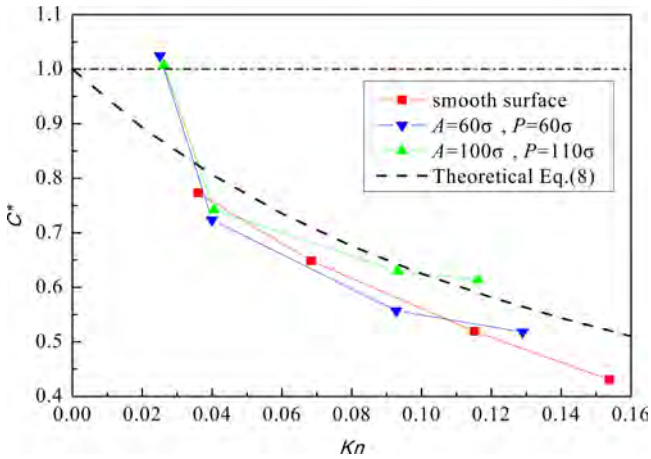

FIG. 12. Friction coefficient C^* varied as a function of Kn when the gas flowed past: a smooth wall (red squares); a permeable bottom wall with nanopores $A = 60\sigma$ and $P = 60\sigma$ (blue inverted triangles); and a permeable bottom wall with nanopores $A = 100\sigma$ and $P = 110\sigma$ (green triangles). The dash-dotted line refers to the no-slip boundary condition.

addition, the friction coefficient C^* on the permeable surface is greater than unity (referring to the no-slip boundary and indicated by the dash-dotted line) for small Kn(= 0.03), resulting from the negative slippage observed in Fig. 9. The theoretical predict of the friction coefficient (indicated by the dashed line) is also shown in Fig. 12 using Eq. (8) with the TMAC (ς) taken equal to unity, and we find that the friction coefficient on the smooth or permeable surfaces is larger than the theoretical one if $Kn > 0.04$. It indicates that the TMAC (ς) deviates from the Maxwellian prediction due to the rarefaction effect and is out of the range of $0 \sim 1.0$. Recently Liakopoulos *et al*. have reported a dependence of the friction coefficient on the geometric characteristics and quantified the associated energy dissipation of nanochannel flow.[48] The energy dissipation consumed by the nanoscale vortices in nanopores is responsible for the large friction coefficient on the permeable surface.

IV. CONCLUSION

This paper has presented the gas nanochannel flow past the permeable walls with nanopores using molecular dynamics (MD) simulations. A three-dimensional Couette flow has been performed to study the influence of the permeable surface on the gas flow in nanochannels. A low density distribution was found at the gas-wall interface indicating the low gas pressure near the wall. In addition, there existed a jump of the gas density on the permeable surface, which indicates the discontinuity of the density distribution when gas molecules crossed the permeable surface into nanopores.

For the dynamics of the gas flow in nanochannels with permeable surfaces, nanoscale vortices were produced in nanopores. The size and number of the vortex in nanopores depended on the size of nanopores. More and large vortices were produced in large nanopores. The mass flux was reduced in nanopores due to the energy dissipation consumed by the nanoscale vortices. As a result, the hydrodynamic boundary had been shifted above the permeable surface. Besides, the slip length on the permeable surface is not a linear function of Kn, which results in a large value of the tangential momentum accommodation coefficient (TMAC) and indicates a big portion of the diffusive refection when the gas molecules impinge on the permeable surface.

Apart from the enhancement of the diffusive reflection, the momentum exchange happened not only between the gas molecules and wall atoms but also between gas molecules themselves in nanopores. It indicates that the gas-gas interactions and multi-collision among gas molecules may take place in nanopores. The small slip length on the permeable surface produced a large friction coefficient, and the energy dissipation caused by the nanoscale vortices in nanopores was responsible for the increase of boundary friction coefficient. The molecular boundary condition on

the smooth wall predicted by Maxwell theory is not suitable for the flow past the permeable surface, and a novel molecular boundary condition is desirable.

ACKNOWLEDGMENTS

The financial support of National Natural Science Foundation of China (Grants No. 51506110 and 51322603) and Science Fund for Creative Research Groups (No. 51321002) for this work was acknowledged. J.F.X also thanks China Postdoctoral Science Foundation (Grant No. 2015M581090) for the support.

[1] J. Koplik and J. R. Banavar, Annual Review of Fluid Mechanics **27**, 257 (1995).
[2] H. Chih-Ming and T. Yu-Chong, Journal of Fluids Engineering - Transactions of ASME **118**, 437 (1996).
[3] H. Chih-Ming and T. Yu-Chong, Annual Review of Fluid Mechanics **30**, 579 (1998).
[4] G.-e.-H. Mohamed, Journal of Fluids Engineering - Transactions of ASME **121**, 5 (1999).
[5] B.-Y. Cao, J. Sun, M. Chen, and Z.-Y. Guo, International Journal of Molecular Sciences **10**, 4638 (2009).
[6] R. Daw and J. Finkelstein, Nature **442**, 367 (2006).
[7] H. Craighead, Nature **442**, 387 (2006).
[8] L. Bocquet and P. Tabeling, Lab Chip **14**, 3143 (2014).
[9] D. R. Reyes, D. Iossifidis, P.-A. Auroux, and A. Manz, Analytical Chemistry **74**, 2623 (2002).
[10] M. L. Kovarik, D. M. Ornoff, A. T. Melvin, N. C. Dobes, Y. Wang, A. J. Dickinson, P. C. Gach, P. K. Shah, and N. L. Allbritton, Analytical Chemistry **85**, 451 (2013).
[11] C. T. Culbertson, T. G. Mickleburgh, S. A. Stewart-James, K. A. Sellens, and M. Pressnall, Analytical Chemistry **86**, 95 (2014).
[12] P. A. Thompson and S. M. Troian, Nature **389**, 360 (1997).
[13] P. A. Thompson and M. O. Robbins, Physical Review A **41**, 6830 (1990).
[14] J. Koplik, J. R. Banavar, and J. F. Willemsen, Physics of Fluids A **1**, 781 (1989).
[15] D. L. Morris, L. Hannon, and A. L. Garcia, Physical Review A **46**, 5279 (1992).
[16] F. D. Sofos, T. E. Karakasidis, and A. Liakopoulos, Physical Review E **79**, 026305 (2009).
[17] Y. Chen, C. Zhang, M. Shi, and G. P. Peterson, Applied Physics Letters **100**, 074102 (2012).
[18] B. Y. Cao, M. Chen, and Z. Y. Guo, Applied Physics Letters **86**, 091905 (2005).
[19] A. S. Berman, Journal of Applied Physics **24**, 1232 (1953).
[20] A. S. Berman, Journal of Applied Physics **27**, 1557 (1956).
[21] C. Lee, C. Cottin-Bizonne, A.-L. Biance, P. Joseph, L. Bocquet, and C. Ybert, Physical Review Letter **112**, 244501 (2014).
[22] K. H. Jensen, A. X. C. N. Valente, and H. A. Stone, Physics of Fluids **826**, 052004 (2014).
[23] D. S. Beavers and D. D. Joseph, Journal of Fluid Mechanics **30**, 197 (1967).
[24] J.-T. Jeong, Physics of Fluids **13**, 1884 (2001).
[25] T. K. Vanderlick and H. T. Davis, Journal of Chemical Physics **87**, 1791 (1987).
[26] S. A. Somers and H. T. Davis, Journal of Chemical Physics **96**, 5389 (1992).
[27] K. S. Page and P. A. Monson, Physical Review E **54**, R29 (1996).
[28] H. Zhang, B. J. Zhang, J. W. Lu, and S. Q. Liang, Chemical Physics Letters **366**, 24 (2002).
[29] D. Kim and E. Darve, Physical Review E **73**, 051203 (2006).
[30] H. Hoang and G. Galliero, Physical Review E **86**, 021202 (2012).
[31] G. Z. Ramon, H. E. Huppert, J. R. Lister, and H. A. Stone, Physics of Fluids **25**, 073103 (2013).
[32] S.C.Yang, Microfluid Nanofluid **2**, 501 (2006).
[33] B.-Y. Cao, M. Chen, and Z.-Y. Guo, International Journal of Engineering Science **44**, 927 (2006).
[34] B. Y. Cao, Molecular Physics **105**, 1403 (2007).
[35] J. Sun, Y. L. He, W. Q. Tao, J. W. Rose, and H. S. Wang, Microfluid Nanofluid **12**, 991 (2012).
[36] E. M. Sparrow, G. S. Beavers, and B. A. Masha, Physics of Fluids **17**, 1465 (1974).
[37] G. A. Bird, Ann. Rev. Fluid Mech. **10**, 11 (1978).
[38] G. A. Bird, *Molecular Gas Dynamics and the Direct Simulation of Gas Flows* (Clarendon Press, Oxford, 1994).
[39] M. P. Allen and D. J. Tildesley, *Computer Simulation of Liquids* (Clarendon, Oxford, 1987).
[40] E. Meiburg, Physics of Fluids **29**, 3107 (1986).
[41] T. Li and W. Ye, Commun. Comput. Phys. **15**, 246 (2014).
[42] M. Barisik and A. Beskok, Microfluid Nanofluid **11**, 269 (2011).
[43] G. S. Grest and K. Kremer, Physical Review A **33**, 3628 (1986).
[44] P. A. Thompson and M. O. Robbins, Physical Review Letter **63**, 766 (1989).
[45] I. J.H. and K. J.G., J. Chem. Phys. **18**, 817–829 (1950).
[46] J. Sun, Y. He, W. Tao, X. Yin, and H. Wang, Int. J. Numer. Meth. Engng. **89**, 2 (2012).
[47] S. Kang and Y. K. Suh, Microfluid Nanofluid **7**, 337 (2009).
[48] A. Liakopoulos, F. Sofos, and T. E. Karakasidis, Microfluid Nanofluid **20**, 24 (2016).
[49] N. Tretyakov and M. M¨uller, Soft Matter **9**, 3613 (2013).
[50] V. P. Sokhan and N. Quirke, Physical Review E **78**, 015301 (2008).
[51] G. Finger, J. Kapat, and A. Bhattacharya, Journal of Fluids Engineering -Transations ASME **129**, 31 (2007).
[52] B.-Y. Cao, J.-F. Xie, and S. S. Sazhin, Journal of Chemical Physics **134** (2011).
[53] W.-L. Li, J.-W. Lin, S.-C. Lee, and M.-D. Chen, Journal of Micromechanics and Microengineering **12**, 149 (2002).